# SPECTRAL ANALYSIS OF SLAT COVE FLOW

**André dos Santos Bonatto, andre.bonatto@poli.usp.br**
**Stergios Pericles Tsiloufas, stergios.tsiloufas@poli.usp.br**
**Rafael dos Santos Gioria, rafaelgioria@yahoo.com.br**
**Julio Romano Meneghini, jmeneg@usp.br**
NDF, Department of Mechanical Engineering, Poli, University of São Paulo, Brazil

**Bernardo Santos Aflalo, bernardo.aflalo@embraer.com.br**
Embraer - Empresa Brasileira de Aeronáutica S.A., São José dos Campos, Brazil

***Abstract.*** *In order to identify noise sources from a leading edge slat and investigate its spectral characteristics, the Koopman Operator Decomposition method is proposed. Results from a time-accurate two-dimensional simulation past MDA 30P30N wing profile are used to compute the eigenvalues and eigenvectors of the discrete version of the Koopman Operator with an Arnoldi Algorithm. Analysis of most energetic modes revealed that most low frequency oscillations are associated with Kelvin-Helmholtz instability mechanisms in the slat shear layer. Moreover, a higher frequency mode in the shear layer is closely related with deformation of the structures in the reattachment region and their convection towards the slat trailing edge.*

***Keywords:*** *Dynamic mode decomposition, Aero-acoustics, Slat noise*

## 1. INTRODUCTION

Airframe noise has emerged as an important problem to aircraft manufacturing industry because noise requirements gradually becomes more stringent. Since flyover measurements of Chow et al. (2002), the leading edge slat has been identified as a prominent noise source and in the following years, much attention in the scientific community was directed towards simulation and identification of slat noise sources. In recent years, the 30P30N geometry has been the focus of aero-acoustics investigations by NASA. Since 2004, when the experiments of Jenkins et al. (2004) were carried out for the validation of two-dimensional time-accurate simulations of Khorrami et al. (2004) there was a large number of attempts of reproducing slat cove dynamics, e.g. Choudhari et al. (2006), Lockard et al. (2009) and more recently Bonatto et al. (2010). Although many authors have successfully captured slat cove dynamics, see for instance Lockard et al. (2009), the identification methods usually rely on correlation and coherence analysis of pressure signals. Decomposition methods are powerful methods to isolate structures of the flow field, giving more details of vorticity dynamics and sound generation. The Fourier Transform Method is good to isolate tonal frequencies of the flow but it is not a recommended method to isolate frequencies in broadband phenomena, such as the noise generated in the slat cove. Proper orthogonal decomposition (POD) method can capture the most energetic modes, but spectral information could easily be lost since each mode could contain several frequencies.

The Koopman Operator Decomposition is a frequency-based method for decomposition of any non-linear flow (Rowley et al., 2009) easy to code and with great potential as a noise source identification tool. Since the method relies only on observed variables, it can be applied to any flow field regardless of Mach and Reynolds numbers, periodicity and linearity. Its general formulation can also be used as a framework for analyzing the interaction of vorticity and pressure fields and its implications for airframe noise.

The main purpose of this work is to assess the capability of Koopman Operator Decomposition (KOD) to isolate flow structures related to noise sources from high-lift devices. Instead of tackling the problem with a high fidelity three-dimensional time-accurate simulation, this paper will only focus on major trends expected from a two-dimensional simulation in order to check the viability of the method as a noise source identification tool.

In section 2 the main properties of the method are briefly presented. In section 3. the simulation methodology is presented, and in the section 4, the Koopman decomposition is applied and the acoustic results are discussed.

## 2. KOOPMAN OPERATOR DECOMPOSITION

### 2.1 Properties of the Koopman modes

The algorithm used to perform the decomposition of the flow into global modes based on the Koopman operator is detailed in Rowley et al. (2009). For sake of consistency, we briefly discuss some important properties of Koopman Operator algorithm in this section.

Let us assume a finite-dimension dynamical system of the form:

$$\mathbf{x}_{k+1} = \mathbf{f}\left(\mathbf{x}_k\right) \tag{1}$$

where $\mathbf{f}$ is the operator that relates the instantaneous state $(k+1)$ of the dynamical system with the previous state $(k)$. The Koopman operator is a infinite-dimensional linear operator constructed from the map $\mathbf{f}$ with the following relation:

$$Ug(\mathbf{x}) = g(\mathbf{f}(\mathbf{x})) \tag{2}$$

where $\mathbf{g}$ is a vector-valued observable of the flow state. The observable could be any flow state measured at interest regions.

If one assume that components of $\mathbf{g}$ lie within the span of the eigenfunctions of U, it can be expanded into a infinite linear combination of the eigenfunctions $\phi_j$ (Koopman modes) of U, which coincide with the eigenvectors of $\mathbf{f}$ for linear systems. It is interesting to notice that if dynamics are restricted to any attractor of the operator $\mathbf{f}$, the Koopman modes coincide with the discrete Fourier transform of finite-time data sets. Thus, Koopman modes analysis could provide a unified approach for treating both linear and periodic non-linear systems. Moreover, Rowley et al. (2009) showed that the Arnoldi algorithm not only could be used to compute Koopman modes of linear systems but also provides a connection to non-linear modal decomposition. This important property is discussed in the following section.

### 2.2 Numerical algorithm

Restricting the analysis to linear systems of the form:

$$\mathbf{x}_{k+1} = \mathbf{A}\mathbf{x}_k \tag{3}$$

it is evident that solving directly the eigenvalue problem for large systems is impractical. A useful solution to estimate these eigenvalues is the Arnoldi algorithm , which takes an initial vector $\mathbf{x}_0$ and the its next $m-1$ iterates to span the Krylov subspace $\{\mathbf{x}_0, \mathbf{A}\mathbf{x}_0, \ldots, \mathbf{A}^{m-1}\mathbf{x}_0\}$. One can project $\mathbf{A}$ onto this $m$-dimensional subspace and find approximate eigenvectors and eigenvalues of the original operator.

We can define the $n \times m$ matrix

$$\mathbf{K} = [\ \mathbf{x}_0 \quad \mathbf{A}\mathbf{x}_0 \quad \ldots \quad \mathbf{A}^{m-1}\mathbf{x}_0\ ] = [\ \mathbf{x}_0 \quad \mathbf{x}_1 \quad \ldots \quad \mathbf{x}_{m-1}\ ] \tag{4}$$

and try to write the $m$-th iterate $\mathbf{x}_m$ as a linear combination of the previous iterates. Generally, we have

$$\mathbf{x}_m = c_0\mathbf{x}_0 + \ldots + c_{m-1}\mathbf{x}_{m-1} + \mathbf{r} = \mathbf{K}\mathbf{c} + \mathbf{r} \tag{5}$$

where $\mathbf{c} = (c_0, \ldots, c_{m-1})$ and $\mathbf{r}$ is a residual, which is minimized when $\mathbf{c}$ is chosen to make $\mathbf{r} \perp \text{span}\{\mathbf{x}_0, \ldots, \mathbf{x}_{m-1}\}$.

It can be shown that

$$\mathbf{A}\mathbf{K} = \mathbf{K}\mathbf{C} + \mathbf{r}\mathbf{e}^T \tag{6}$$

where $\mathbf{e} = (0, 0, \ldots, 0, 1) \in \mathbb{R}^m$ and $\mathbf{C}$ is a companion matrix given by

$$\mathbf{C} = \begin{bmatrix} 0 & 0 & \ldots & 0 & c_0 \\ 1 & 0 & & 0 & c_1 \\ 0 & 1 & & 0 & c_2 \\ \vdots & & \ddots & & \vdots \\ 0 & 0 & \ldots & 1 & c_{m-1} \end{bmatrix}. \tag{7}$$

One can show that the eigenvalues of $\mathbf{C}$ are a subset of the eigenvalues of $\mathbf{A}$, called Ritz values. If $\mathbf{C}\mathbf{a} = \lambda\mathbf{a}$, then $\mathbf{v} = \mathbf{K}\mathbf{a}$ is an eigenvector of $\mathbf{A}$ with eigenvalue $\lambda$.

We are now ready to provide the connection between linear and non-linear analysis. In Rowley et al. (2009) it was showed that if we apply this algorithm to the first $m$ snapshots from a set of $m+1$ collected from simulation or experiment data, then the last snapshot could be approximated by the linear expansion:

$$\mathbf{g}(\mathbf{x}_m) = \sum_{i=1}^{m} \lambda_i^m \mathbf{v_i} + \mathbf{r} \tag{8}$$

Hence if we collect $m$ snapshots $\mathbf{x}_0, \ldots, \mathbf{x}_{m-1}$separated by the time interval $\Delta t$ , one can obtain approximation of the Koopman modes $\mathbf{V} = \mathbf{K}\mathbf{T}^{-1}$, where $\mathbf{T}^{-1}$ is the matrix with eigenvectors of $\mathbf{C}$ as columns and $f = arg\left(\dfrac{\lambda_i}{2\pi\Delta t}\right)$ is the frequency of the Koopman mode.

Given that $\mathbf{r}$ in equation 8 is constructed to be orthogonal to the span of the dataset, when $||\mathbf{r}|| = 0$, the Ritz values and the corresponding modes are the best approximation to spectrum of the Koopman operator. However, if $||\mathbf{r}|| \neq 0$, then the residual is the smallest possible error in projecting $\mathbf{g}(\mathbf{x}_m)$ onto the vector space generated by the previous $m$ snapshots.

## 3. FLOW FIELD DESCRIPTION AND SIMULATION METHODOLOGY

The experimental data used as a benchmark for the present computations were recorded for the following flow condition: angle of attack of $4°$, $\mathrm{Re} \approx 1.7 \times 10^6$ and $\mathrm{M} \approx 0.17$ for a model with stowed chord of 0.457 meters and inflow velocity of $56m/s$. A detailed description of the experimental apparatus can be found in the original reference (Jenkins et al., 2004). Although all elements had finite thickness, in our study only the slat trailing edge thickness ($h \approx 0.36mm$) was maintained, while the main element and flap trailing edges were sharpened to avoid the need of a fine grid resolution in those areas.

The computational simulations were performed for a free-flight configuration with angle of attack of $5.5°$, which closely approximates the $4°$ wind tunnel flow over the wing model (Khorrami et al., 2004). Version 8.1.2 of CFD++ software suite was used to solve the compressible time-dependent Navier-Stokes equations in a two-dimensional multiblock overset grid containing a total of 484,919 nodes, with 137,975 points covering the slat cove (see Fig. 1). Second-order upwind method was used for the spatial discretization, with second-order point wise implicit time integration. Ten subiterations of dual time-stepping algorithm with pseudo-time-derivative preconditioning technique was used to guarantee at least three orders of magnitude of residual drop. Characteristic boundary conditions were imposed in the far-field boundaries, while at solid surfaces no-slip conditions and adiabatic wall boundary conditions were applied. The two-equation $k - \omega$ Shear Stress Transport model of Menter was used in the whole simulation domain, except at the slat cove, where the turbulence source term was switched off in order to capture shear layer unsteadiness (Bonatto et al., 2010).

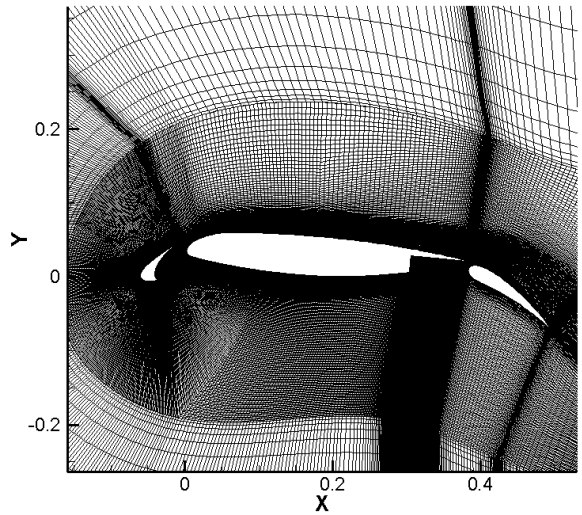


Figure 1. Grid distribution over the wing model.

A note of caution is needed regarding turbulence modeling. It was earlier reported that conventional URANS modeling could suppress shear layer instabilities (Khorrami et al., 2003). A comprehensive study of turbulence models and their effect on high-lift devices simulations is beyond the purposes of this paper. For the interested reader, those issues are discussed in the papers of Aflalo et al. (2010) and Bonatto et al. (2010).

It should be highlighted that two-dimensional simulations may not provide a suitable representation of the physical experiment, specially when the flow regime is well beyond the critical Reynolds number for spanwise instabilities. Unfortunately, this is exactly the case of the this benchmark case. Khorrami et al. (2004) attributed the differences between computation and measurements to three-dimensionality effects. Nonetheless, one can expect that some major characteristics of the flow, such as vortical structures, are greatly influenced by the 2D wing geometry. In this case, the Koopman Operator Decomposition can act as a preliminary noise source identification tool.

Furthermore, significant differences were also found in three-dimensional simulations of Choudhari et al. (2006) and Lockard et al. (2009), attributed to the spanwise extent of the simulations. A comprehensive verification of simulations would require studies of mesh convergence, sensitiveness to spanwise length, boundary layer resolution and time-step, which would exceed a practical time to check if the decomposition can capture sound sources and waves.

## 4. RESULTS

Figure 2(b) shows a snapshot of instantaneous vorticity contours, in which it is possible to notice the continuous roll-up of the shear layer due to Kelvin-Helmholtz instability mechanism and the vortex impingement in the slat pressure surface. In order to test the ability of the method to capture only most energetic structures in the flow field, we used 400 snapshots of the oscillatory flow (i.e. the mean flow is subtracted from each snapshot) in the same domain shown in Fig. 2.

Sampling period is $\Delta t = 1 \times 10^{-5}$.

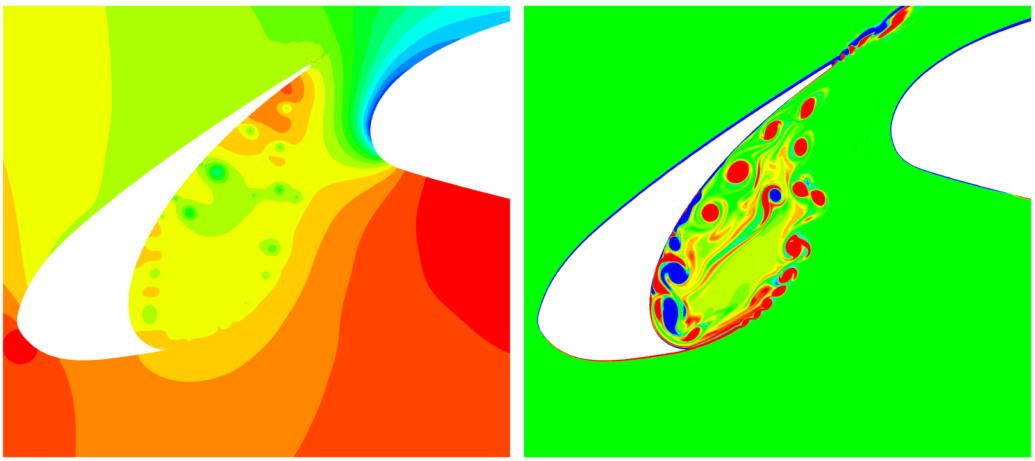

(a) (b)

Figure 2. Instantaneous contours for base flow in slat cove region. (a) Pressure (79 to 89 kPa). (b) Spanwise vorticity ($-10000$ to $10000\ \mathrm{s}^{-1}$).

In Fig. 3(a) we can see the eigenvalues of the Koopman Operator and, as expected for a developed flow field, most of them lie on unit circle. Looking at the spectrum (Figures 3(b) and 3(c)) one can notice that the modes with greater energy are the ones with low frequency, because these modes characterize the cove dynamics. In higher frequencies one can observe some small peaks, which can be studied as dynamic modes of interest in sound generation.

In this work we studied three modes, including the low frequency ($f \approx 1250$Hz) shear layer undulation mode, observed in Figs. 4(a) and 4(b) in terms of spanwise vorticity and acoustic pressure contours. This analysis clearly shows that the shear layer instability does not radiate a great amount of acoustic energy. Therefore, another mechanism for the broadband noise radiation should be sought.

The second mode studied is the one with $f \approx 5500$Hz and its topology is shown in Figs. 4(c) and 4(d). This mode presents the shear layer divided into two trains of vortices : the large-scale vortices present only in the shear layer and the small-scale structures present near the shear layer and in the vicinity of slat surface, both in the recirculation zone and the trailing edge. Comparing this mode with the instantaneous vorticity contours, it can be noticed that the structures near the trailing edge from the second mode have scales comparable to the trailing edge vortices. Therefore, one may infer that acoustic wave is created by the interference between this shear layer mode in the slat pressure side with trailing edge vortices. This mode is associated with the shear layer Kelvin-Helmholtz instability, and another interesting structure emerges in the reattachment region as vortices are split. Some vortices get trapped in the recirculation region and some are convected towards the trailing edge, generating the acoustic wave. This result is very promising since authors in Khorrami et al. (2004) identified a high level of unsteadiness in this region but they were unable to recognize the frequency of ejection of vortices.

The higher frequency ($f \approx 29,000$Hz) mode studied in this work is associated with the vortex shedding pattern both in the trailing edge and in the cusp of the slat, as it can be seen in Figs. 4(e) and 4(f). Although two acoustic waves are identified, each one emerging from one of the vortex shedding regions, the stronger acoustic structure is created in the slat trailing edge. This is an expected result since the waves emanating from the cusp are reflections of the waves emitted at the trailing edge.

Distinct patterns from modes 2 and 3 indicates that in this flow condition, the trailing edge frequency is isolated from the corresponding mode of the cove shear layer. As it can be seen, the shear layer mode decays so fast that there is not enough energy for disturbing the shedding at the trailing edge. Comparing now modes 1 and 2, it is clearly seen that only a selected number of modes do radiate from the slat. The topology of mode 2 indicates pulsating flow in the impingement and trailing edge regions and, while mode 1 does not have intense patterns at the trailing edge and no sound radiation. Moreover, the vorticity structures leaving the slat cove are much more oriented towards spanwise direction in the radiating mode than the corresponding structures in the non-radiating mode.

## 5. CONCLUSION AND FUTURE ACTIVITIES

The Koopman modes decomposition method is a promising method for noise source identification in high lift systems. Although one can question the validity of the physical solution using the two-dimensional simulations, the KOD method has been successfully tested and proved itself useful in separating the flow features into frequencies modes. The authors expect that with better input snapshots, which can be provided from three-dimensional simulations or experiments, via

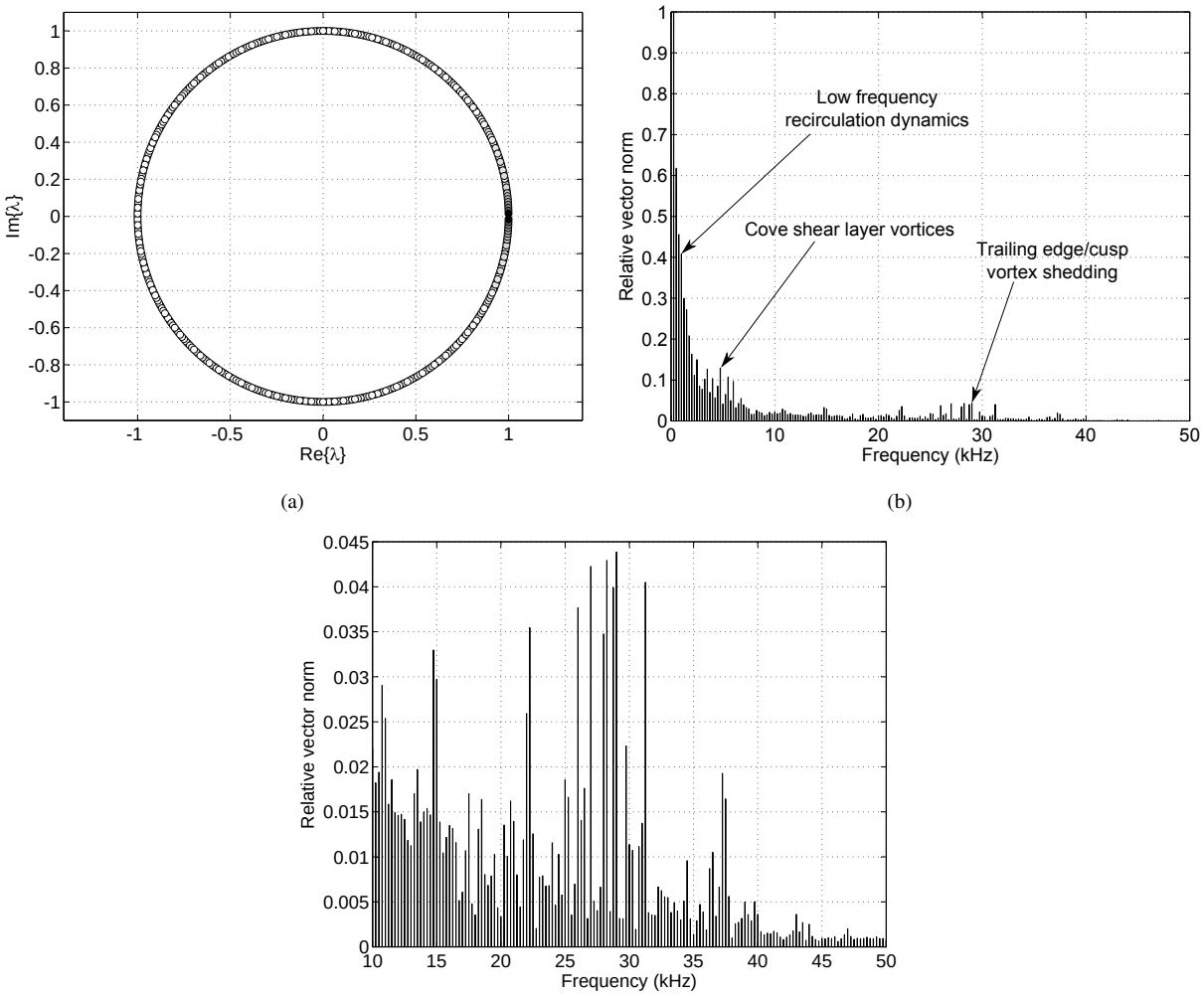


Figure 3. (a) The empirical eigenvalues $\lambda$. Color varies from white to black, depending on the magnitude of the corresponding mode. (b) Relative magnitudes of the Koopman modes, except the zero frequency mode. (c) Same as (b), focusing on $10$ kHz to $50$ kHz frequency range.

particle image velocimetry, the method would be able to identify the correct sound sources and propagating waves. In this paper, it has been successfully applied to isolate structures emanating from the slat cove region even with moderate levels of unsteadiness in other areas such as the flap cove.

The broadband nature of the problem, specifically the presence of a decaying mode and a stable one with distinct frequencies in the reattachment point makes it difficult to recognize spectral characteristics of the flow field with a simple visualization of the snapshots as done earlier in the literature. The KOD method was able to isolate shear layer frequencies, corresponding to radiating and non-radiating modes.

Although we limited our analysis to three modes of two vorticity and pressure, it was shown that only structures oriented in the spanwise direction do radiate pressure disturbances to the farfield. This radiating mode is not only related to the continuous process of shear layer roll-up and emission of vortices but also related to large pressure disturbances at the slat trailing edge. Therefore, the method presented in this work can potentially be applied to isolate mechanisms dominating the sound radiation from the large number of non-radiating shear layer modes.

Future studies intend to expand the analysis to three-dimensional simulations in order to allow a direct comparison with experiments and spectral correlations presented in the literature. This analysis which will require, for computational limitations, the input snapshots to be limited only to the region of interest.

## 6. ACKNOWLEDGEMENTS

We would like to acknowledge the financial support provided by Fapesp, CNPq, and Embraer. All the computing resources were provided by NDF - University of São Paulo.

## 7. REFERENCES

B.S. Aflalo, L.G.C. Simões, R.G. Silva and M.A. Medeiros, 2010, "Comparative analysis of turbulence models for slat noise sources calculations employing unstructured meshes". AIAA Paper 3838.

A.S. Bonatto, V.M.L. Lopes, J.R. Meneghini and F. Saltara, 2010, "Comparative analysis of turbulence models for slat noise sources calculations employing structured meshes". AIAA Paper 3834.

M.M. Choudhari and M.R. Khorrami, 2006, "Slat Cove Unsteadiness: Effect of 3D Flow Structures". AIAA Paper 0211.

L.C. Chow, K. Mau and H. Remy, 2002, "Landing Gears and High Lift Devices Airframe Noise research". AIAA Paper 2408.

L.N. Jenkins, M.R. Khorrami and M. Choudhari, 2004, "Characterization of unsteady flow. Structures near leading-edge slat. Part I: PIV measurements". 10th AIAA/CEAS Aeroacoustics Conference and Exhibit.

M. Khorrami, M. Choudhari, B. Singer, D. Lockard and C. Streett, 2003, "In Search of the Physics: The Interplay of Experiment and Computation in Slat Aeroacoustics". AIAA Paper 0980.

M. Khorrami, M. Choudhari and L.N. Jenkins, 2004, "Characterization of Unsteady Flow Structures Near a Leading-Edge Slat: Part II. 2D Computations". AIAA Paper 2802.

D.P. Lockard and M. Choudhari, 2009, "Noise radiation from a leading edge slat". AIAA Paper 3101.

C.W. Rowley, I. Mezic, S. Bagheri, P. Schlatter and D.S. Henningson, 2009, "Spectral analysis of nonlinear flows". Journal of Fluid Mechanics, Vol. 641, pp. 115–127.

## 8. RESPONSIBILITY NOTICE

The author(s) is (are) the only responsible for the printed material included in this paper

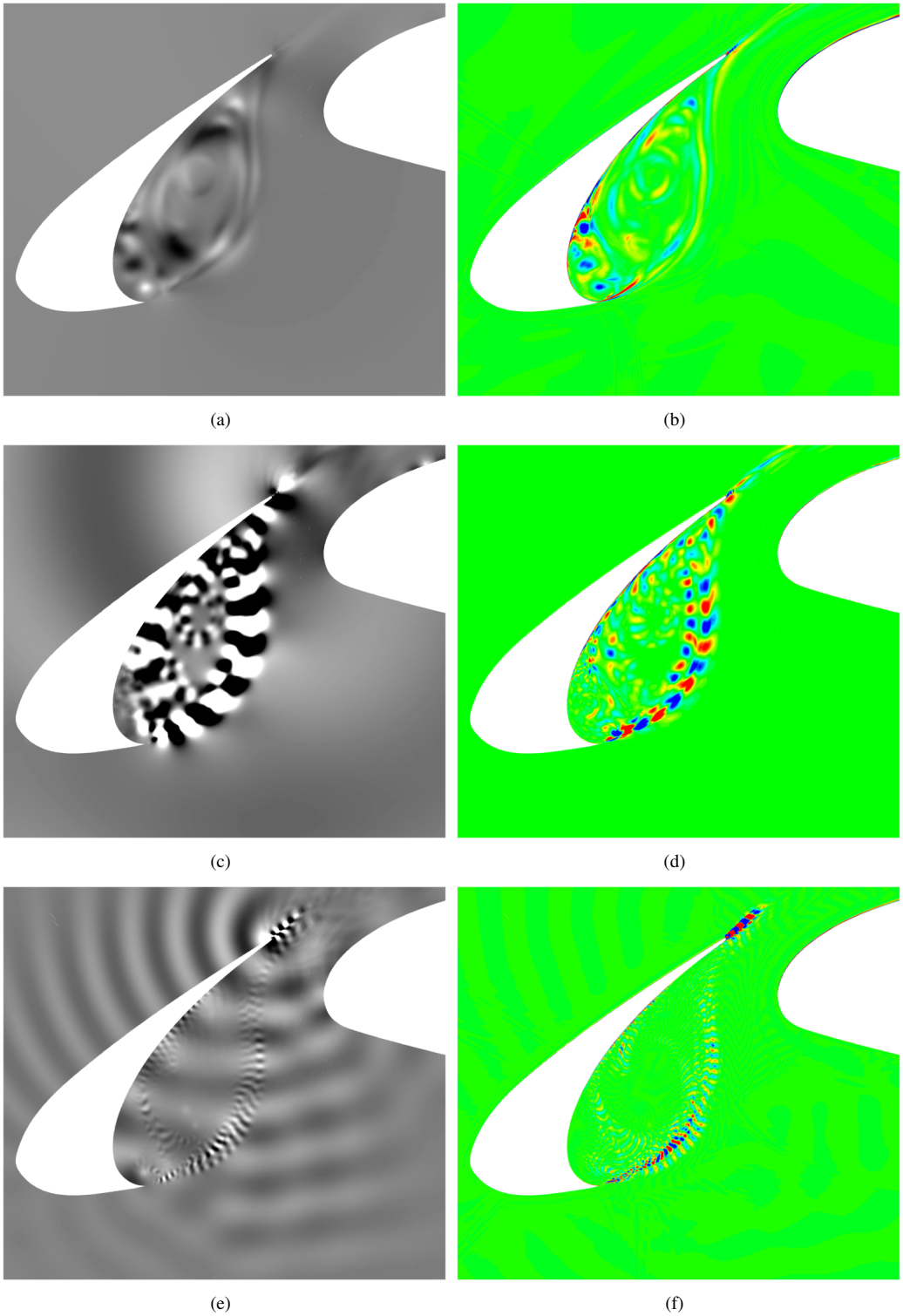


Figure 4. (a), (c), (e) Acoustic pressure contours. (b), (d), (f) Spanwise vorticity contours. (a), (b) Low frequency recirculation dynamics, $f \approx 1250\,\mathrm{Hz}$. (c), (d) Cove shear layer vortices, $f \approx 5500\,\mathrm{Hz}$. (e), (f) Trailing edge and cusp vortex shedding, $f \approx 29,000\,\mathrm{Hz}$..